Armenian Journal of Physics, 2023, vol. 16, issue 1, pp. 13-19

Continuous Metal-Insulator Transition and Scale Laws in Metallic n-Type InP

D. Ennajih[1], H. Mabchour[1], A. El kaaouachi[2,*], A. Echchelh[1], A. El oujdi[1], E. Mounir[1], B. Ait Hammou, S. Dlimi[3]

[1] *Laboratory of Energetic Engineering and Materials, Faculty of Sciences Ibn Tofail, Kenitra, Morocco.*
[2]*Physics department, Faculty of Sciences of Agadir, BP 8106, 80000 Agadir, Morocco.*
[3]*Laboratory of LSTIC, Physics Department, Faculty of Sciences, Chouaib Doukkali, El jadida, Morocco.*

Email:kaaouachi21@yahoo.fr

(Received: March 30, 2023; Revised: April 21, 2023; Accepted: May 4, 2023)

Abstract. We have studied the transport properties in metallic n-type InP semiconductor. We show that the dependence on temperature of metallic electrical conductivity obey to the law $\sigma = \sigma(T = 0) + mT^{1/2}$. We highlight the absence of a minimum electrical conductivity σ_{min} proposed by Mott at the metal-insulator transition. We show that the conductivity at temperature T = 0 *K*, $\sigma(T = 0)$, follows a scaling law as a function of the effective parallel and perpendicular Bohr radii $a_{\|}$ and $a_{\perp}$.

Keywords: metallic side of Metal-Insulator Transition, low temperatures, strong magnetic, scale theory, effective parallel and perpendicular Bohr radii $a_{\|}$ and $a_{\perp}$

DOI:10.54503/18291171-2023.16.1-13

1. Introduction

In this paper the low-temperature electrical properties of an n-type InP device in the metallic regime of the metal-insulator transition (MIT) are studied in the presence of magnetic fields. The impurity concentration is $n=1.23\cdot10^{23}m^{-3}$ with a compensation parameter $k=0.5$, the carrier concentration has been determined from measurements of the Hall coefficient at room temperature and the compensation was determined by the method described by Brooks [1].The critical concentration n_c in InP is calculated to $5\cdot10^{22}m^{-3}$ using the Mott criterion [2, 3] ($n_c^{1/3}a_H=0.25\pm0.05$) with the dielectric constant of 12.5.This indicates that our sample falls on the metallic side of the MIT. The experiments are carried out at low temperature (between 0.066 K and 4.2 K) and in magnetic fields up to *11 T*. The InP sample is driven to the MIT by applying a strong magnetic field. All the physical parameters of our sample are grouped in Table1.

It is well known that in three dimensions on the metallic side of the MIT, the electrical conductivity σ can be fitted by the following equation

$$\sigma = \sigma(T = 0) + mT^s, \tag{1}$$

where the exponent *s* can be calculated to be 0.5 or 0.33 [4-7], where, $\sigma(T = 0)$ is the conductivity at $T = 0$ *K*, *T* is the temperature, *m* is the coefficient of thermal variation. *s* and *m* are adjustable parameters. The fitting procedure was as follows: *s* was varied from 0.01 to 1 with steps in 0.01; for each value of *s* the data were fitted to equation (1). $\sigma(T = 0)$ and *m* were obtained by the standard linear regression methods. The quality of the fit was tested with the estimation of the percentage deviation

$$Dev(\%) = \left[\frac{1}{p}\sum_{i=1}^{p}\left(\frac{100}{\sigma_i}((\sigma_0 + mT^s) - \sigma_i)\right)^2\right]^{1/2}, \tag{2}$$

where σ_i are the experimental values of the electrical conductivity at different temperatures.

Table 1. Physical parameters of our InP sample.

Parameter	**Symbol**	**Value**
Effective mass	$\frac{m^*}{m_0}$	0.079
Dielectric constant	ε	12.5
Impurity concentration	n	$1.2310^{23}m^{-3}$
Fermi vector	k_F	$1.542710^{8}m^{-1}$
Fermivelocity	V_F	$2.2596\ m/s$
Fermi energy	E_F	$1.83810^{-21}J$
Free Pathmean	l_0	$148.4410^{-10}m$
Elastic diffusion time	τ	$6.5710^{-14}s$
Diffusion constant	D	$11.18210^{-4}m^2/s$

In Fig. 1 we plot *Dev(%)* against the exponent *s* for values of the magnetic field. It is clear that the exponent *s* is almost equal to 0.5. We find the same result for all the other values of the magnetic field. In Fig. 2 we plot the electrical conductivity σ against $T^{1/2}$ for several magnetic fields.

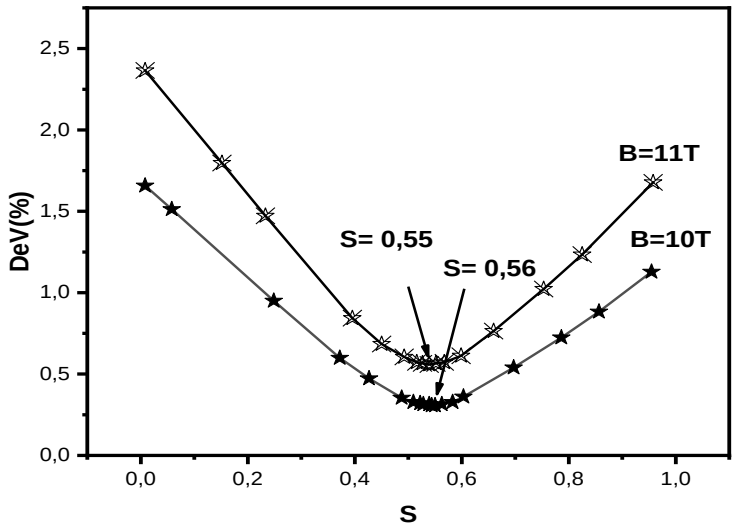

Fig. 1. Percentage deviation in Eq. (2) *Dev(%)* versus exponent *s* in Eq. (1) for two values of magnetic fields (for *B=10 T, S=0.56* and for *B=11 T, s =0.55*). The exponent *s* is very close to *0.5*.

In Fig. 3 we plot *σ(T = 0)* obtained by the standard linear regression method of the curves σ against $T^{1/2}$ versus magnetic field *B*. We note that *σ(T = 0)* decreases linearly when the magnetic field increases. *σ(T = 0)* tends to zero for *B ≈15.2T*. This shows that a minimum electrical conductivity σ_{min} proposed by Mott [2, 3] at the MIT do not exist in this sample and that the MIT is done continuously. This MIT must occur at a critical magnetic field $B_c \approx 15.2T$. B_c forms de boundary between the metallic (*B<15.2 T*) and the insulating (*B>15.2 T*) sides of MIT.

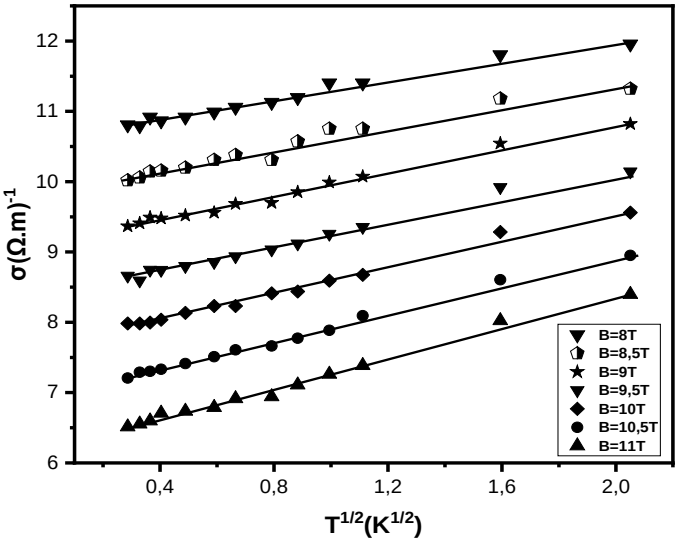

Fig. 2. Electrical conductivity σ against $T^{1/2}$ for several values of strong magnetic fields.

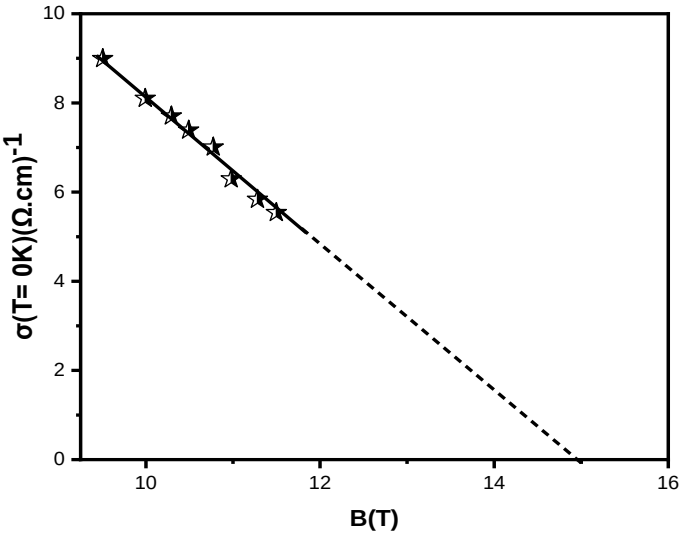

Fig. 3. *σ(T = 0K)* versus magnetic field *B*.

2. Determination of effective parallel and perpendicular Bohr radii $a_{\parallel}$ and $a_{\perp}$

In this paragraph we will calculate an effective parallel and perpendicular Bohr radii $a_{\parallel}$ and $a_{\perp}$($a_{\parallel c}$ and $a_{\perp c}$ are their critical value at the MIT). We use the normalized wave function given by [8] as function as $a_{\parallel}$ and $a_{\perp}$

$$\varphi = (2^{\frac{3}{2}} {a_{\perp}}^2 a_{\parallel} \pi^{\frac{3}{2}})^{-1/2} exp\left[-\frac{(x^2+y^2)}{4{a_{\perp}}^2} - \frac{z^2}{4{a_{\parallel}}^2}\right], \quad (3)$$

x, y, z being the coordinates along the X, Y and Z axis.

Yafet [8] poses

$$E = \langle \varphi | H | \varphi \rangle, \quad (4)$$

where *E* is the ionization energy and *H* is the Hamiltonian of the moving atom with the presence of a uniform magnetic field. Using Eq. (4) we obtain

$$E = \frac{1}{2{a_\perp}^2}\left(1+\frac{\epsilon^2}{2}\right) + \frac{\gamma^2 {a_\perp}^2}{2} - \frac{\epsilon\sqrt{2}}{a_\perp\sqrt{\pi(1-\epsilon^2)}} ln\left[\frac{1+\sqrt{1-\epsilon^2}}{1-\sqrt{1-\epsilon^2}}\right], \quad (5)$$

with γ *is* a dimensionless quantity given by $\gamma = \frac{\hbar w_c}{2R_\gamma}$. $w_c = \frac{eB}{m^*}$ is a cyclotron frequency. R_γ is the Rydberg constant and $\epsilon = \frac{a_\perp}{a_\parallel}$.

By minimizing *E* we obtain

$$\frac{\delta E}{\delta \epsilon} = 0, \quad (6)$$

and

$$\frac{\delta E}{\delta a_\perp} = 0. \quad (7)$$

We obtain

$$\frac{\delta E}{\delta \epsilon} = \frac{\epsilon}{2{a_\perp}^2} + \frac{1}{a_\perp}\sqrt{\frac{2}{\pi}}\left[\frac{2}{(1-\epsilon^2)}\right] + \left\{-\frac{1}{\sqrt{(1-\epsilon^2)}} - \frac{\epsilon^2}{(1-\epsilon^2)^{3/2}}\right\} ln\left[\frac{1+\sqrt{1-\epsilon^2}}{1-\sqrt{1-\epsilon^2}}\right] = 0, \quad (8)$$

$$\frac{\delta E}{\delta a_\perp} = -\frac{1}{{a_\perp}^3}\left(1+\frac{\epsilon^2}{2}\right) + \gamma^2 a_\perp + \frac{\epsilon\sqrt{2}}{a_\perp\sqrt{\pi(1-\epsilon^2)}} ln\left[\frac{1+\sqrt{1-\epsilon^2}}{1-\sqrt{1-\epsilon^2}}\right] = 0. \quad (9)$$

By using Eq. (8) we obtain

$$a_\perp = -\frac{\epsilon}{2h(\epsilon)} \quad , \quad (10)$$

with

$$h(\epsilon) = \sqrt{\frac{2}{\pi}}\left[\frac{2}{(1-\epsilon^2)} + \left\{-\frac{1}{\sqrt{(1-\epsilon^2)}} - \frac{\epsilon^2}{(1-\epsilon^2)^{3/2}}\right\} ln\left[\frac{1+\sqrt{1-\epsilon^2}}{1-\sqrt{1-\epsilon^2}}\right]\right]. \quad (11)$$

By using Eq. (9) we obtain

$$\left(\frac{2h(\epsilon)}{\epsilon}\right)^3\left(1+\frac{\epsilon^2}{2}\right) + \gamma^2\left(\frac{-\epsilon}{2h(\epsilon)}\right) + \left(\frac{2h(\epsilon)}{\epsilon}\right)^2 + \left[\frac{\epsilon\sqrt{2}}{\sqrt{\pi(1-\epsilon^2)}} \ln\left[\frac{1+\sqrt{1-\epsilon^2}}{1-\sqrt{1-\epsilon^2}}\right]\right] = 0. \quad (12)$$

Eq. (11) can be written as

$$F(\epsilon, \gamma) = 0. \quad (13)$$

By calculatingγ for each magnetic field we obtain a function $F(\epsilon)$ with only one variable. For each fixed magnetic field, we search numerically for the root of the function $F(\epsilon) = 0$. Each time we numerize and draw the function $F(\epsilon)$, and we determine graphically the value of ϵ which cancels the function $F(\epsilon)$. In Fig. 4 we present an overview of the function $F(\epsilon)$ for a fixed magnetic field. Once ϵ, we calculate the function $h(\epsilon)$ by using Eq.(11).$a_\perp$is obtained using Eq. (10) and $a_\parallel$ is calculated using the relation $\epsilon = \frac{a_\perp}{a_\parallel}$.

In Fig. 5 we plot an effective parallel and perpendicular Bohr radii $a_\parallel$ and $a_\perp$ versus the parameter $\gamma(\gamma = \frac{\hbar w_c}{2R_\gamma})$.

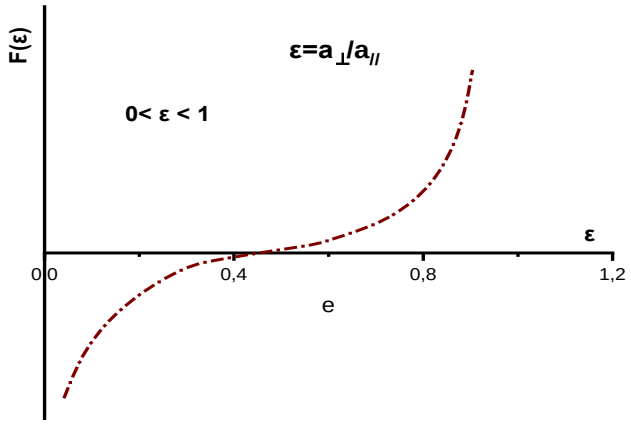

Fig. 4. Overview of the function $F(\epsilon)$ for a fixed magnetic field *B*.

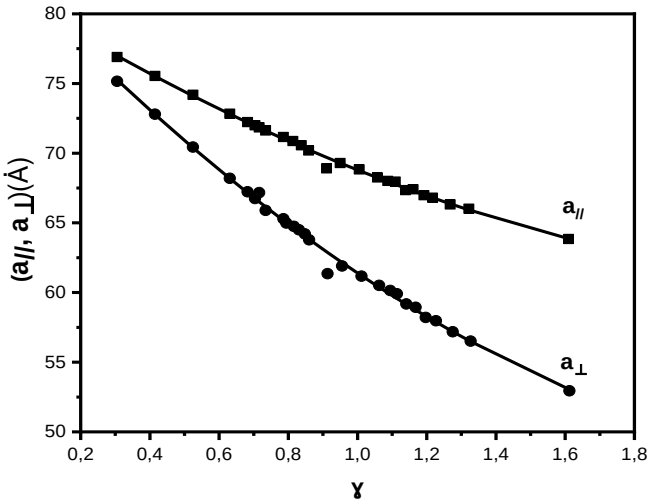

Fig. 5. Variation of an effective parallel and perpendicular Bohr radii $a_{\parallel}$ and $a_{\perp}$ versus parameter γ.

3. Scale law relating $\sigma(T = 0)$ to effective parallel and perpendicular Bohr radii $a_{\parallel}$ and $a_{\perp}$

Several authors have emitted different theories based on the renormalization equations and their derivatives to establish scaling laws that the conductivity at zero temperature $\sigma(T = 0)$ could satisfy. Abrahams et.al. [9] have denied the existence of minimum conductivity σ_{min} at the MIT in systems where electron-electron interactions do not exist. This was confirmed experimentally in doped semiconductors [10-14]. Scale laws have been verified experimentally by several researchers [15], who shown that $\sigma(T = 0K) = \sigma_C\,(\frac{n}{n_C} - 1)^{\nu}$ with the exponent ν equal to 1 or $1/2$.When the sample is driven to MIT by applying a strong magnetic field $\sigma(T = 0K)$ obey to the following scale law $\sigma(T = 0K) = \sigma_C\,(1 - \frac{B}{B_C})^{\nu}$.

Another approach to the variation of $\sigma(T = 0K)$ with magnetic field is to use a scale law in which is introduced the Mott criterion ($n_c^{1/3}\ a_H$=0.25±0.05) dependent on the magnetic field through the effective parallel and perpendicular Bohr radii $a_{\parallel}$ and $a_{\perp}$.We obtain

$$\sigma(T = 0K) = \sigma_C\,(\frac{{a_{\perp}}^2 a_{\parallel}}{{a_{\perp c}}^2 a_{\parallel c}} - 1)^{\nu}. \qquad (14)$$

In Fig. 6 we plot $\ln(\sigma(T=0\,K))$ against $ln(\frac{{a_\perp}^2 a_\parallel}{{a_{\perp c}}^2 a_{\parallel c}}-1)$. We notice that $\sigma(T=0\,K)$ verifies the scale law given by Eq. (14). We obtain $\sigma_C = 16.94(\Omega cm)^{-1}$ and $\nu = 0.87$. This value obtained for the exponent ν is appreciably close to 1. This result is in good agreement with theories.

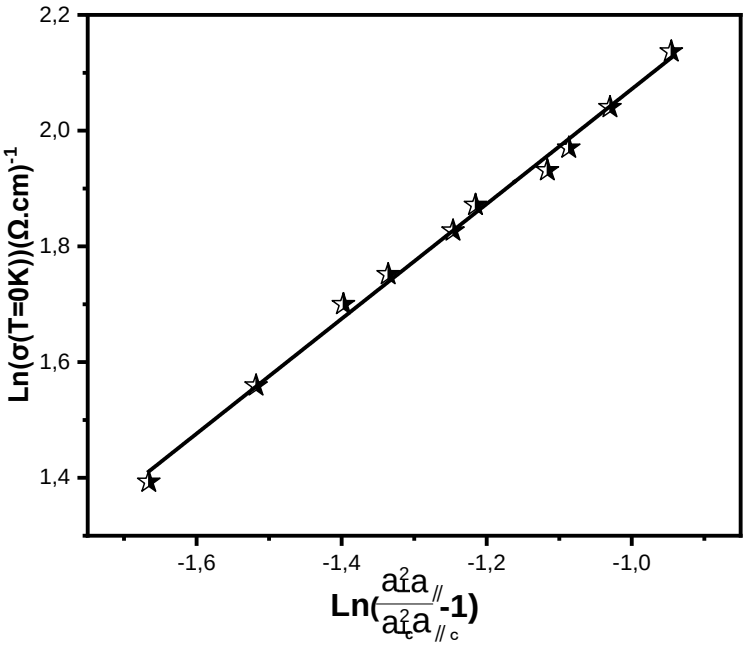

Fig. 6. $\ln(\sigma(T=0K))$ versus $ln(\frac{{a_\perp}^2 a_\parallel}{{a_{\perp c}}^2 a_{\parallel c}}-1)$.

4. Conclusions

In this work, we have shown using a numerical method of the percentage deviation *Dev(%)* given by Eq. (2), that the electrical conductivity in metallic side of the MIT obey to the law $\sigma = \sigma(T=0) + mT^{0.5}$. We have also shown that this MIT is done continuously and that the minimum electrical conductivity σ_{min} at the MIT suggested by Mott does not exist in our sample. We have also shown that the conductivity at zero temperature *σ(T = 0)* follows a scale law as function as the effective parallel and perpendicular Bohr radii $a_\parallel$ and $a_\perp$. In previous works we have study the behaviors of electrical conductivity in the both sides of the MIT in 2D and 3D systems [16-23]. We shown that the MIT can be driven by applying strong magnetic fields or by varying the concentration of impurities, and that the electrical conductivity follows a Variable Range Hopping conduction regime according to Mott or according to Efros–Schklovskii in the insulating side of the MIT. We have also shown that the behavior of the electrical conductivity in metallic side of the MIT is due to the weak localization effects, the electron-electron interactions effects and the Zeeman effect in the presence of a magnetic field.

References

[1] H. Brooks, Adv. Electron. Electron Phys. **7** (1955) 158.
[2] N.F. Mott, Phil. Mag. **26** (1972) 1015.
[3] N.F. Mott, Phil. Mag. **6**(1961) 287.
[4] M.C. Maliepaard, M. Pepper, R. Newbury, Phys. Rev. Lett. **61** (1988) 369.
[5] D.J. Newson, M. Pepper, J. Phys. C: Sol. Stat. Phys. **19** (1986) 3983.
[6] B.L. Altshuler, A.G. Aronov, JETP Lett. **37** (1983) 410.

[7] A. Sybous, A. El kaaouachi, A. Ait Ben Ameur, B. Capoen, J. Hemine, R. Abdia, A. Narjis, H. Sahsah, G. Biskupski, J. Phys. B: Condens. Matt. **406** (2011) 3489.
[8] Y. Yafet, R.W. Keyes, E.N. Adams, J. Phys. Chem. Solids **1** (1956) 137.
[9] E. Abrahams, P.W. Anderson, D.C. Lucciardelo, T.V. Ramakrishnan, Phys. Rev. Lett. **42** (1979) 673.
[10] A. El kaaouachi, N. Ait Ben Ameur, B. Capoen, R. Abdia, A. Narjis, A. Sybous, G. Biskupski, Proc. SPIE **7758** (2010) 775805.
[11] M. Errai, A. El kaaouachi, H. El idrissi, J. Semiconductor (IOP) **36** (2015) 1.
[12] M. Errai, S. Amrane, E3S Web of Conf. **229** (2021) 01056.
[13] A. El oujdi, S. Dlimi, A. Echchelh, A. El kaaouachi, Phys. Sol. Stat. **62** (2020) 2445.
[14] T.F. Rosenbaum, K. Andres, G.A. Thomas, R.N. Bhatt, Phys. Rev. Lett. **45** (1980) 1723.
[15] A. Sybous, A. El kaaouachi, A. Narjis, L. Limouny, S. Dlimi, G. Biskupski, Proc. Phys. Chem. Interfaces and Nanomaterials XI **8459** (2012) 84590W.
[16] A. Narjis, A. El kaaouachi, L. Limouny, S. Dlimi, A. Sybous, J. Hemine, R. Abdia, G. Biskupski, J. Phys. B **406** (2011) 4155.
[17] S. Dlimi, A. El kaaouachi, A. Narjis, L. Limouny, A. Sybous, M. Errai, J. Phys. Chem. Sol. **74** (2013) 1349.
[18] A. Narjis, A. El kaaouachi, G. Biskupski, E. Daoudi, L. Limouny, S. Dlimi, M. Errai, A. Sybous, J. Mat. Sci. Semicond. Proc. **16** (2013) 1257.
[19] M. Errai, A. El kaaouachi, H. El idrissi, A. Chakhmane, Chin. J. Phys. **55** (2017) 2283.
[20] A. Chakhmane, H. El idrissi, A. El kaaouachi, M. Errai, J. Korean Phys. Soc. **75** (2019) 389.
[21] S. Dlimi, A. EL kaaouachi, L. Limouny, J. Appl. Surf. Sci. Advances **3** (2021) 100045.
[22] L. Limouny, S. Dlimi, A. El kaaouachi, Bull. Mat. Sci. **44** (2021) 210.
[23] M. El Hassan, S. Dlimi, L. Limouny, A. El oujdi, A. Echchelh, A. El kaaouachi, J. Mol. Cryst. Liq. Cryst. **726** (2021) 82.